



City Research Online

City, University of London Institutional Repository

Citation: Ferreira, F. P. V., Shamass, R., Santos, L. F. P., Tsavdaridis, K. D. & Limbachiya, V. (2023). Web-Post Buckling Prediction Resistance for Perforated High-Strength Steel Beams with Elliptically-Based Web Openings. *Structures*, 55, pp. 245-262. doi: 10.1016/j.istruc.2023.05.139

This is the accepted version of the paper.

This version of the publication may differ from the final published version.

Permanent repository link: <https://openaccess.city.ac.uk/id/eprint/30569/>

Link to published version: <https://doi.org/10.1016/j.istruc.2023.05.139>

Copyright: City Research Online aims to make research outputs of City, University of London available to a wider audience. Copyright and Moral Rights remain with the author(s) and/or copyright holders. URLs from City Research Online may be freely distributed and linked to.

Reuse: Copies of full items can be used for personal research or study, educational, or not-for-profit purposes without prior permission or charge. Provided that the authors, title and full bibliographic details are credited, a hyperlink and/or URL is given for the original metadata page and the content is not changed in any way.

City Research Online:

<http://openaccess.city.ac.uk/>

publications@city.ac.uk

Web-post buckling resistance for perforated high-strength steel beams with elliptically-based web openings

Felipe Piana Vendramell Ferreira^{a*}, Rabee Shamass^b, Luis Fernando Pinho Santos^b,
Konstantinos Daniel Tsavdaridis^c, Vireen Limbachiya^b

^aFederal University of Uberlândia, Faculty of Civil Engineering – Campus Santa Mônica, Uberlândia, Minas Gerais, Brazil

^bLondon South Bank University, School of Built Environment and Architecture, London, UK

^cDepartment of Engineering, School of Science and Technology, City, University of London, Northampton Square, EC1V 0HB, London, UK

**Corresponding author*

Abstract

There has been an increase in the use of high-strength steel in several countries, as they provide design lightweight structural members by satisfying environmental and economic issues. This paper aims to implement high-strength steels in the web-post buckling resistance equation, which was based on the truss model according to EUROCODE 3, presented previously by the authors. For this task, a finite element model is developed by geometrically and materially nonlinear analysis with imperfections included. A parametric study is carried out, considering the key geometric parameters that influence the web-post buckling resistance. Three high-strength steel grades are studied (S460, S690 and S960) and in total, 13,500 finite element models are processed. A new factor for adapting high-strength steels to the equation proposed previously was presented. The finite element results agree well with the new proposal. The statistical parameters calculated, via the ratio between the numerical and analytical models, considering the

regression, mean, standard deviation and variance, were 0.9817, 0.986, 8.32% and 0.69%, respectively. In conclusion, a reliability analysis was presented based on Annex D EN 1990 (2002).

Keywords: High-strength steel; Elliptically-based web openings; Finite element method; Web-post buckling; Reliability analysis.

E-mail addresses:

fpvferreira@ufu.br (F. P. V. Ferreira)

shamassr@lsbu.ac.uk (R. Shamass)

pinhosl3@lsbu.ac.uk (L. F. P. Santos)

konstantinos.tsavdaridis@city.ac.uk (K. D. Tsavdaridis)

limbachv@lsbu.ac.uk (V. Limbachiya)

Notation

The following notations and symbols are used in this paper:

b_f	the flange width;	k	Coefficient in Eq. (2);
d	the parent section height;	K	Coefficient in Eq. (9);
d_g	the total height after castellation process;	K_{HSS}	Coefficient in Eq. (13);
d_o	the opening height;	l_{eff}	the web-post effective length;
d_t	the tee height;	R	the opening radius;
$f_{cr,w}$	the critical shear stress in the web-post;	s	the web-post width;
f_y	the yield strength of the steel section;	t_f	the flange thickness;
f_u	the ultimate stress of the steel section;	t_w	the web thickness;
h	the distance between flanges geometric centres of the parent section;	V	the global shear;
H	the distance between flanges geometric centres after castellation process;	w	the opening width;
		ε	strain;
		λ_o	the reduced slenderness factor;
		λ_w	the web-post slenderness factor;
		σ	stress;
		χ	the reduction factor;

1. Introduction

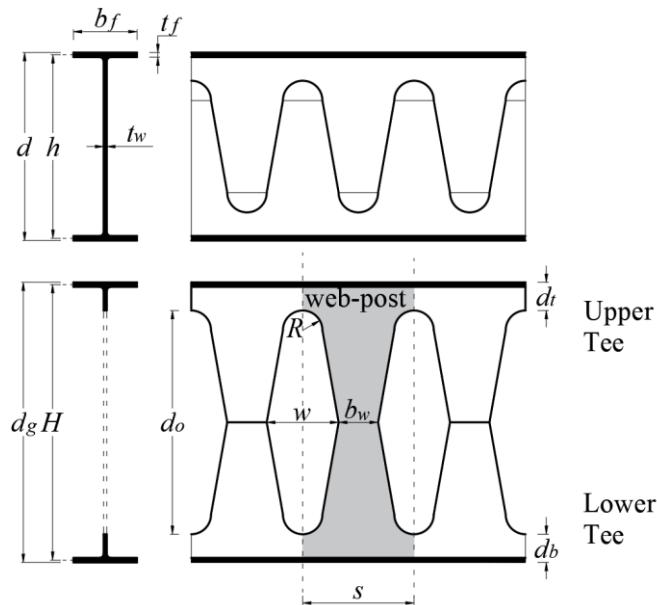
Steel beams with elliptically-based periodical web openings are manufactured by the castellation process¹ (**Fig. 1**). They present several advantages in construction buildings, highlighting the flexural stiffness due to the castellation process, the reduction in the structure's self-weight with the addition of multiple closely spaced periodical web openings, reduction in the structural floor height since the openings allow the passage of ducts for service integration and favors the flow of air in closed environments such as underground parking [1,2].

However, due to the presence of adjacent web openings and long spans, those beams can reach different buckling modes, i.e., lateral-torsional, web-post, web distortional, local flange and web, or even the interaction between them [3–6]. The present study focuses on the web-post buckling. It is a local web buckling mode with double curvature characterised by a lateral displacement with torsion due to the horizontal shear acting in the web-post [7,8]. In general, the main geometric parameters that influence the web-post buckling resistance of perforated beams are the opening height, the web-post width, and the web thickness [9,10].

Studies of steel beams with elliptically-based web openings started with Tsavdaridis [11] and subsequently, several results were published. Tsavdaridis and D'Mello [12,13] and Tsavdaridis et al. [14] worked with optimization problems considering various shapes of openings. These studies

¹Cutting and welding process based on increasing of the cross-section height, and consequently the flexural stiffness. This process is described in the patent GB 2492176 that was published by Tsavdaridis and D'Mello [18].

23 highlighted that elliptically-based web openings resisted the formation of
 24 plastic hinges at low values of loading. Tsavdaridis and D’Mello [8] carried
 25 out tests considering different web openings shapes. The beams were
 26 subjected to three-point bending. This investigation showed that elliptically-
 27 based web openings had greater resistance to horizontal shear which caused
 28 the web-post buckling. In Tsavdaridis and D’Mello [15], an optimisation study
 29 was conducted to assess the Vierendeel mechanism resistance. The authors
 30 emphasized that the elliptical-based web openings showed an increase in the
 31 flexural stiffness, i.e., lower deflections when compared to steel beams with
 32 circular web openings. Ferreira et al. [16] presented a web-post buckling
 33 resistance calculation procedure focused on EC3 [17] strut model. This
 34 procedure is presented in section 2.



35
 36 Fig. 1: Steel beams with elliptically-based web openings [18]

37 All previous studies employed normal strength steels, such as S275 and
 38 S355. High-strength steels (HSS) are those with a yield strength (f_y) greater
 39 or equal to 460 MPa. The application of HSS has been increasing in several

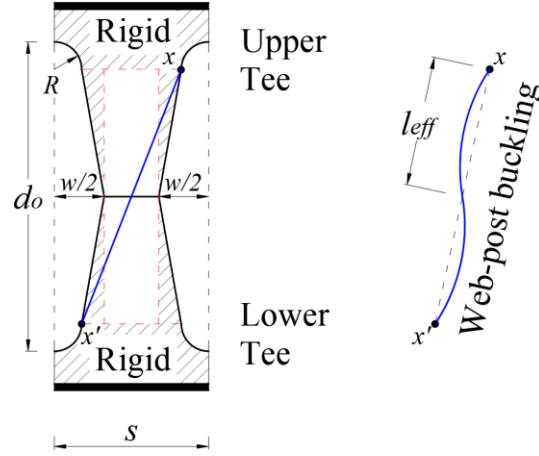
40 countries, mainly due to economic and environmental issues, since less
41 material is used to perform the same functions as normal strength steels, as
42 well as possess an increased corrosion resistance leading to durability and
43 low maintenance [19–24]. The application of HSS makes the design of
44 lightweight structures possible by achieving substantial weight savings
45 where 34% savings had been recorded [25]. This paper aims to investigate the
46 web-post buckling resistance of steel beams with elliptically-based web
47 openings made of HSS. For this task, a finite element model is developed and
48 calibrated with tests by buckling and post-buckling analyses using Abaqus
49 [26]. A parametric study is conducted considering three classes of high-
50 strength steel, such as S460, S690 and S960. A Python script is written to
51 automate the high volume of analyses and a total of 13,500 finite element
52 models are developed. The results are discussed and a proposal is made for
53 design focus.

54

55 **2. Web-post buckling resistance of perforated steel beams with** 56 **elliptically-based web openings**

57 The calculation procedure, which is presented here, is based on the
58 compressed truss model (**Fig. 2**), according to EC3 [17], considering buckling
59 curves. In this scenario, SCI P355 [27] recommends using the buckling curves
60 b and c for hot-rolled and welded sections, respectively. Although these
61 recommendations are directed to perforated steel beams with circular web
62 openings, it is possible to apply them to steel beams with elliptical-based web
63 openings, since these structures are also manufactured by the castellation

64 process (similar to cellular beams), taking into account thermal cutting and
 65 welding.



66

67 Fig. 2: Compressed truss model [16]

68 According to Ferreira et al. [16], the web-post buckling resistance is
 69 calculated considering **Eqs. (1-10)**, in which l_{eff} is the web-post effective
 70 length, d_o is the opening height, R is the opening radius, H is the distance
 71 between flanges geometric centres after castellation process, s is the web-post
 72 width, w is the opening height, λ_w is the the web-post slenderness factor, t_w is
 73 the web thickness, $f_{cr,w}$ is the critical shear stress in the web-post, f_y is the
 74 yield strength, λ_o is the reduced slenderness factor and χ is the reduction
 75 factor. Although the web-post buckling resistance results presented by these
 76 equations were accurate in the previous study, it is important to highlight
 77 that high-strength steels had not been considered.

$$l_{eff} = k \sqrt{\left(\frac{d_o - 2R}{2}\right)^2 + \left(\frac{s}{2} - R\right)^2} \quad (1)$$

$$k = 0.516 - 0.288 \left(\frac{H}{d_o}\right) + 0.062 \left(\frac{s}{s-w}\right) + 2.384 \left(\frac{s}{d_o}\right) - 2.906 \left(\frac{w}{d_o}\right) \quad (2)$$

$$\lambda_w = \frac{l_{eff}\sqrt{12}}{t_w} \quad (3)$$

$$f_{cr,w} = \frac{\pi^2 E}{\lambda_w^2} \quad (4)$$

$$\lambda_0 = \sqrt{\frac{f_y}{f_{cr,w}}} \quad (5)$$

$$\phi = 0.5[1 + 0.49(\lambda_0 - 0.2) + \lambda_0^2] \quad (6)$$

$$\chi = \frac{1}{\phi + \sqrt{\phi^2 - \lambda_0^2}} \leq 1.0 \quad (7)$$

$$\sigma_{Rk} = K\chi f_y \quad (8)$$

$$K = -1.318 + 1.790\left(\frac{H}{d_o}\right) + 0.413\left(\frac{s}{s-w}\right) - 1.926\left(\frac{s}{d_o}\right) + 0.937\left(\frac{w}{d_o}\right) - 0.02\left(\frac{d_o}{t_w}\right) + 1.412\lambda_0 \quad (9)$$

$$V_{Rk} = \sigma_{Rk} t_w (s - w) \quad (10)$$

78

79 3. Finite element method

80 There are no tests available in the literature in relation to HSS beams
81 with elliptically-based web openings. Hence, a numerical model is developed
82 and validated for beams made of normal strength steel, such as S355 grade.
83 In this context, A1, A2, B1, B2 and B3 tests, which were carried out by
84 Tsavdaridis and D'Mello [8], are used in the validation study. As previously
85 presented by Ferreira et al [16], in the web-post resistance assessment, the
86 finite element models can be validated against tests considering full beam
87 and web-post models. The latter is a methodology consolidated in the
88 literature and has been widely used by several researchers [7,9,16,28–34].

89 Geometrical and material nonlinear analysis with imperfections included
90 (GMNIA) is considered. The initial geometric imperfection is applied with an
91 amplitude of $d_g/500$, as recommended by Panedpojaman et al. [29], since it
92 provided accurate results. A multilinear constitutive model of steel is
93 employed, considering steel S355, as presented in Shamass and Guarracino
94 [35] and Yun and Gardner [36]. The modulus of elasticity and Poisson's
95 coefficient are equal to 200 GPa and 0.3, respectively. It is important to
96 highlight that the development of full beams finite element models allows a
97 comparison between the numerical and test results, i.e., load-displacement
98 relationships. On the other hand, the web-post finite element model only
99 allows numerical validation against test models considering the global shear.

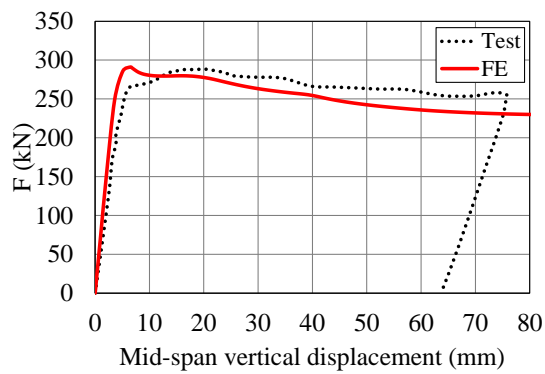
100

101 3.1. Full models

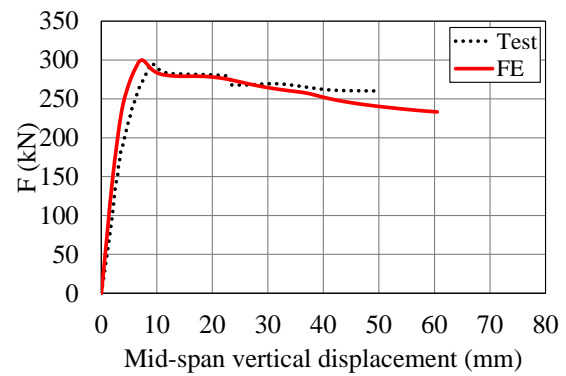
102 Full models of perforated steel beam are modelled, considering 10 mm
103 four-nodes S4R shell elements [16,37–39]. It has four nodes, six degrees of
104 freedom (three rotations and three translations) per node and reduced
105 integration, a factor that reduces processing time. The boundary conditions
106 of the full models were applied according to Ferreira et al. [16]. According to
107 the authors, simply supported beams with lateral restraint at the supports
108 are considered. At the bottom of the stiffener in one end, vertical and
109 longitudinal displacements are restrained ($U_y=U_z=0$). At the bottom of the
110 stiffener in the other end, only the vertical displacement is restrained ($U_y=0$).
111 At both ends, in the region of the stiffeners, lateral displacement and the

112 rotation around the longitudinal axis are restrained at four points
 113 ($U_x=U_{Rz}=0$) [16].

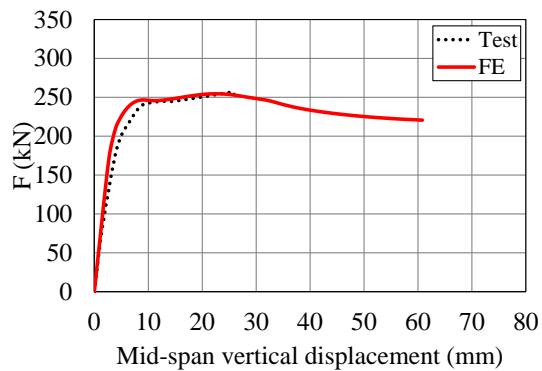
114 The validation results are presented considering load-displacement
 115 relationship (**Fig. 3**), as well as the final configuration (**Fig. 4**). According to
 116 the illustrations, it can be verified that the numerical model of the full models
 117 are validated.



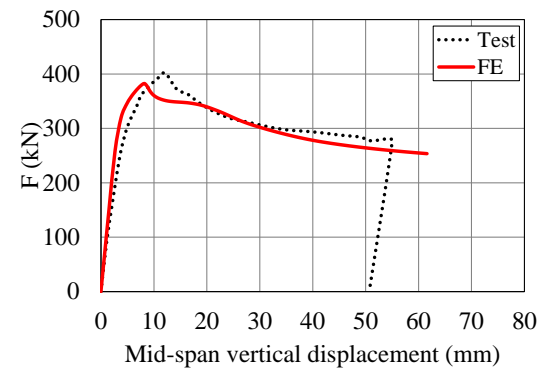
(a) A1



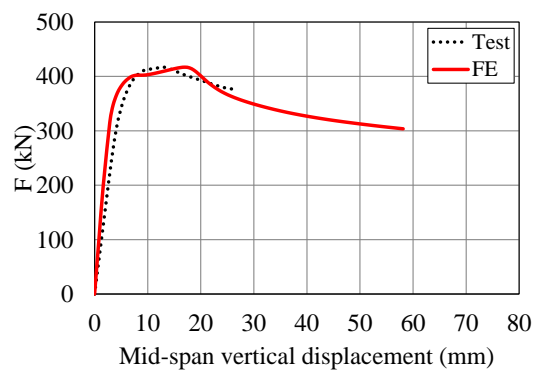
(b) A2



(c) B1



(d) B2



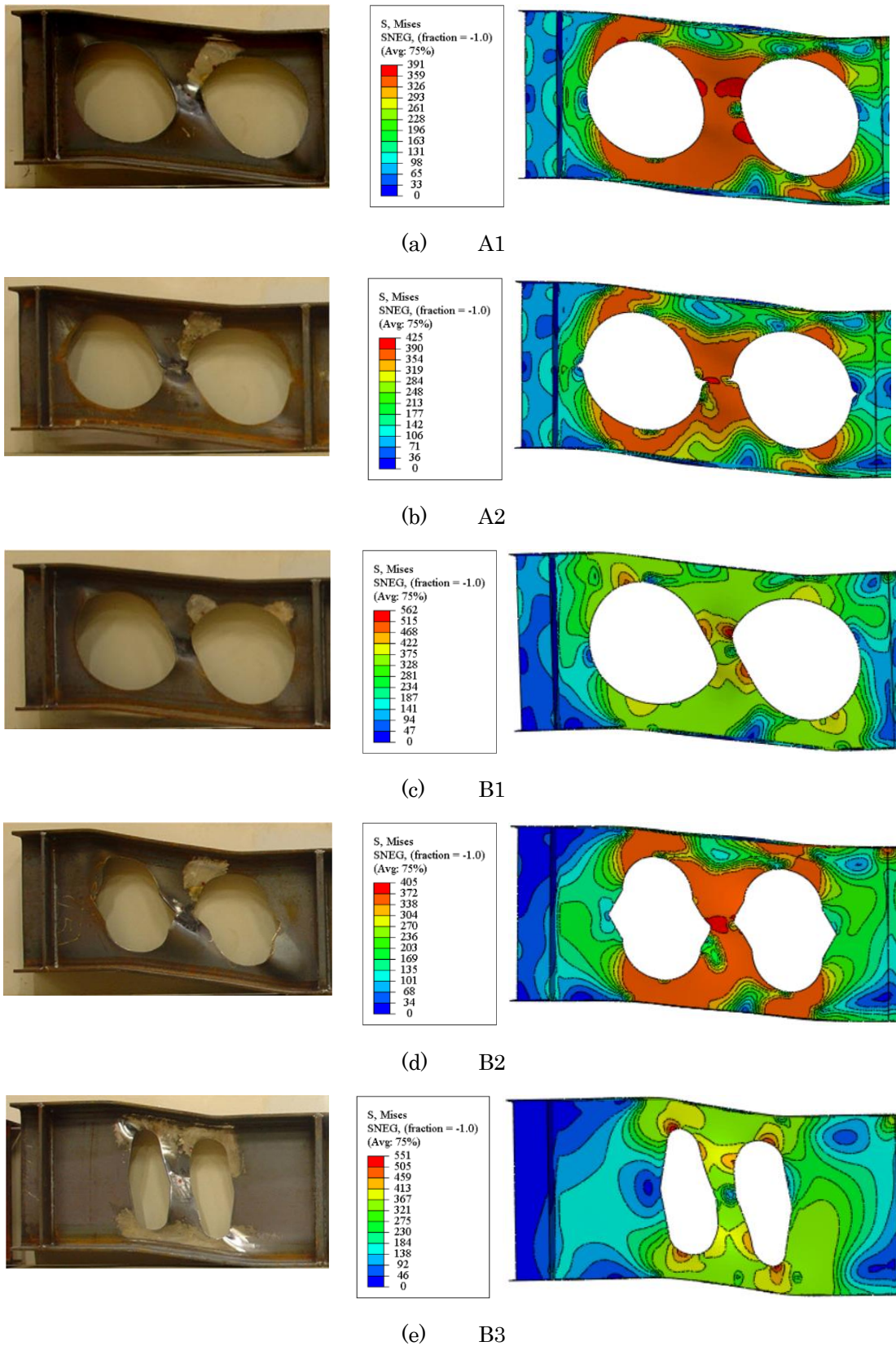
(e) B3

118

Fig. 3: Comparison between tests and finite element models by load-

119

displacement relationships

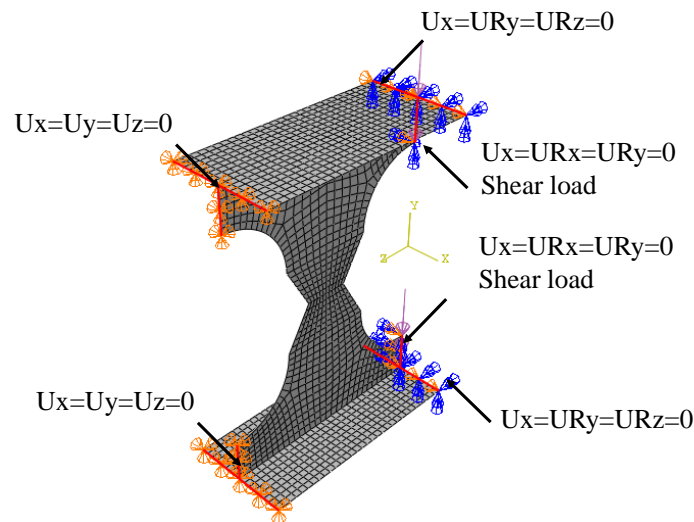


120 Fig. 4: Comparison between tests [8] and finite element models [16] by final
 121 configuration

122

123 3.2. Web-post models

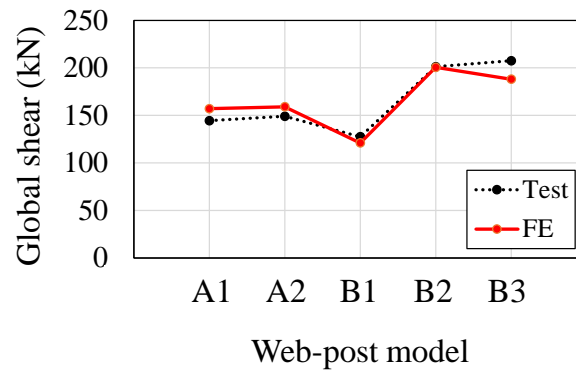
124 Also, the web-post of a perforated steel beam is modelled, considering
 125 S4R shell elements. After several trials and comparisons with the tests
 126 results, the boundary conditions shown in **Fig. 5** were employed, resulting in
 127 adequate predictions. Shear loads were applied along the webs on the tee
 128 sections.



129

130 Fig. 5: Boundary conditions

131 The numerical model results, in comparison with the tests, are
 132 presented in **Fig. 6**. The maximum relative error was 9.4%. The standard
 133 deviation and variance were 6.93% and 0.48%, respectively. In this context,
 134 it is possible to state that the web-post finite element models were adequately
 135 validated. As the main concern of this paper is to investigate the web-post
 136 buckling resistance, a single web-post model is used.



137

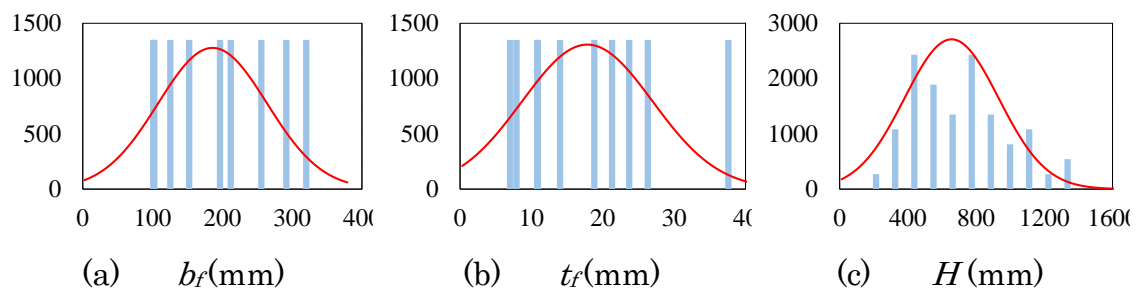
138

Fig. 6: Validation results of web-post models

139

140 4. Parametric study

141 The parametric study presented herein is based on the finite element
 142 validation study described in the previous section. The frequency in function
 143 of the investigated key parameters is illustrated in **Fig. 7**, in particular the
 144 flange width (**Fig. 7a**), the flange thickness (**Fig. 7b**), the distance between
 145 flanges geometric centres after castellation process (**Fig. 7c**), the web
 146 thickness (**Fig. 7d**), the opening height (**Fig. 7e**), the opening width (**Fig. 7f**),
 147 the opening radius (**Fig. 7g**) and high-strength steel grades (**Fig. 7h**). In total
 148 13,500 finite element models are processed, taking into account the key
 149 parameters as illustrated in **Fig. 1**.



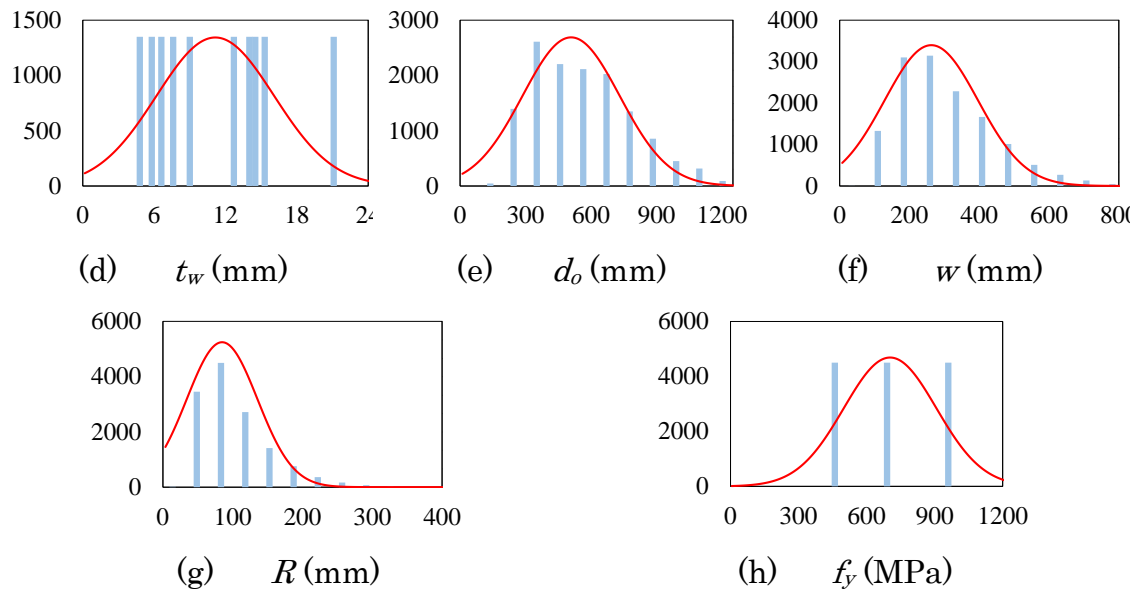


Fig. 7: Frequency based on parameters investigated

150

151 The models in the present parametric study include an eigenvalue
 152 buckling analysis followed by a geometrically nonlinear analysis with
 153 imperfections sympathetic with the first buckling mode and an imperfection
 154 size of $d_g/500$. The geometric nonlinear analysis including imperfections
 155 determines the web-post buckling mode and attains the capacity of the model.
 156 A Python script is developed to conduct the parametric study and post-process
 157 the results and it is available at <https://github.com/luisantos090/WPB>.

158 The script creates a FE model according to the parameters in **Fig. 1** and
 159 the boundary conditions shown in **Fig. 5**. The mesh size discretises the web
 160 with 200 elements over the height and the flanges with 20 elements over the
 161 width. For the largest sections presented in this study, the mesh sizes are 6.7
 162 and 14.6 mm for web and flanges, respectively. The web mesh size follows the
 163 recommendation of using 10 mm or less based on mesh sensitivity studies
 164 referenced previously in the validation study. The script post-processes the
 165 models by storing both the buckling load and the failure mode which are then

166 used to develop and test the proposed new factor for web-post buckling of
 167 high-strength steels.

168

169 5. Results and discussion

170 Some examples of the finite element results that are normalised to the
 171 EC3 buckling curves and presented by Ferreira et al. [16] (**Eqs. 11-14**) are
 172 presented in **Figs. 8-11**, considering the variation of the key geometric
 173 parameters, as well the yield strength, in which $V_{cr,FE}$ and $V_{u,FE}$ are the global
 174 shear predicted by buckling and post-buckling analyses, respectively. From
 175 13,500 finite element models processed, 10,764 models had the resistance
 176 defined by web-post buckling. As the influence of geometric parameters on
 177 capacity has already been discussed in Ferreira et al. [16] considering S355
 178 steel grade, in this section only the analyses referring to high-strength steels
 179 are examined. In this way, the influence of yield strength on web-post
 180 buckling resistance of perforated steel beams with elliptically-based web
 181 openings is discussed briefly considering the key geometric parameters.

$$f_{cr,w,FE} = \frac{V_{cr,FE}}{t_w(s-w)} \quad (11)$$

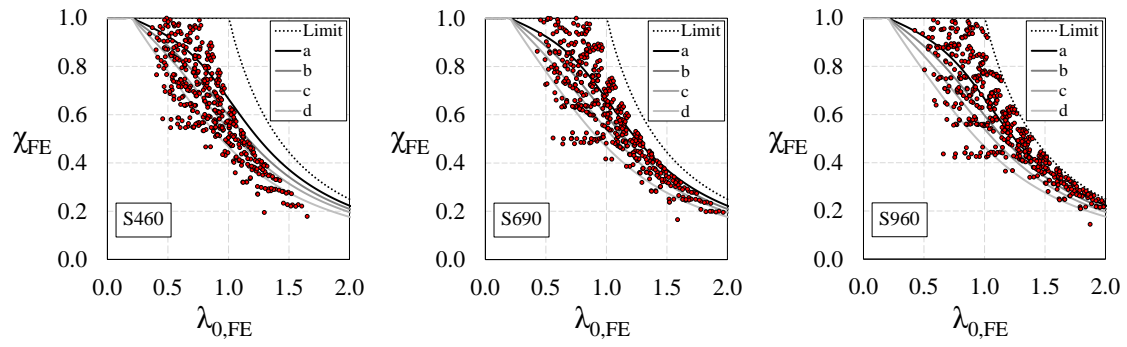
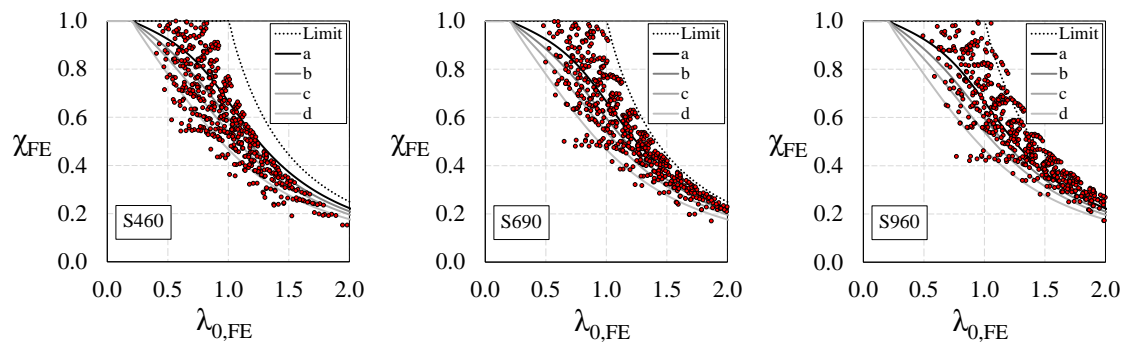
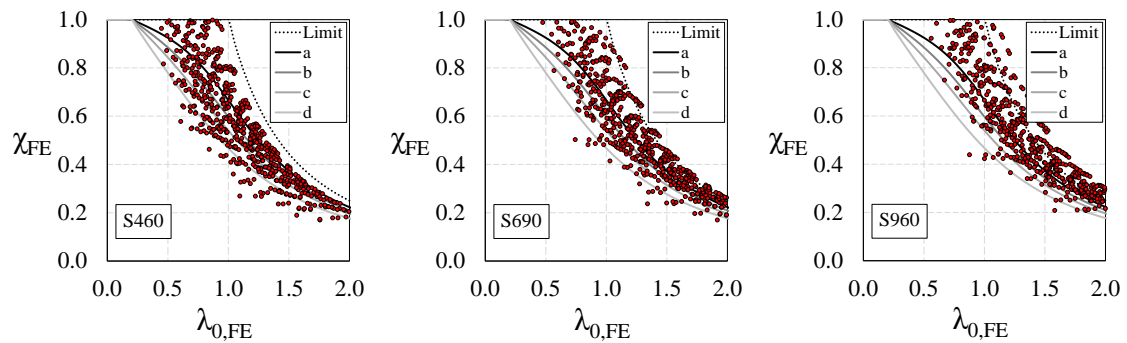
$$\lambda_{0,FE} = \sqrt{\frac{f_y}{f_{cr,w,FE}}} \quad (12)$$

$$\sigma_{u,FE} = \frac{V_{u,FE}}{t_w(s-w)} \quad (13)$$

$$\chi_{FE} = \frac{\sigma_{u,FE}}{f_y} \quad (14)$$

182

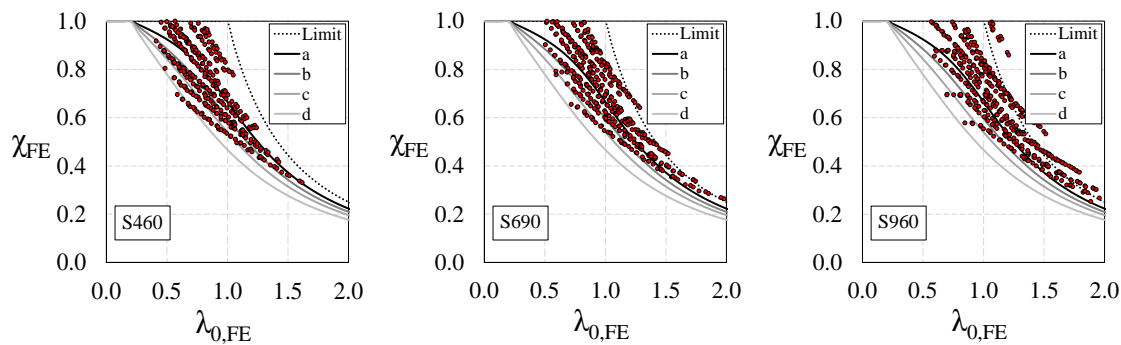
183

(a) $H/d=1.2$ (b) $H/d=1.4$ (c) $H/d=1.6$

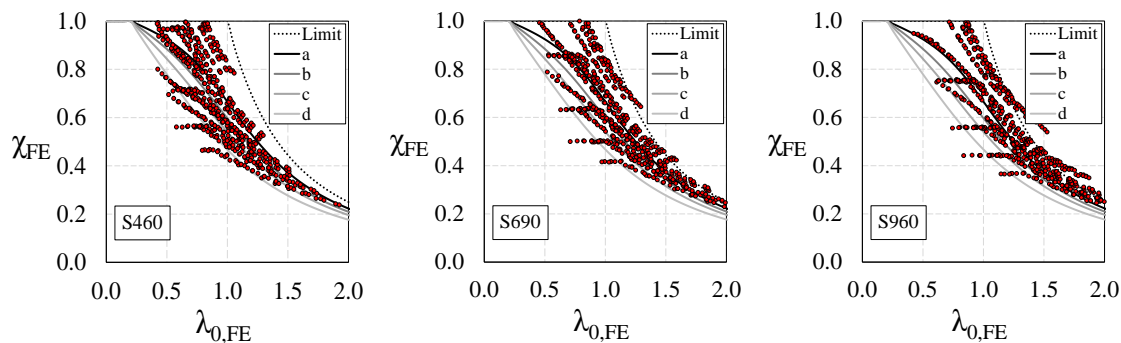
184

Fig. 8: H/d ratio vs. buckling curves of EC3

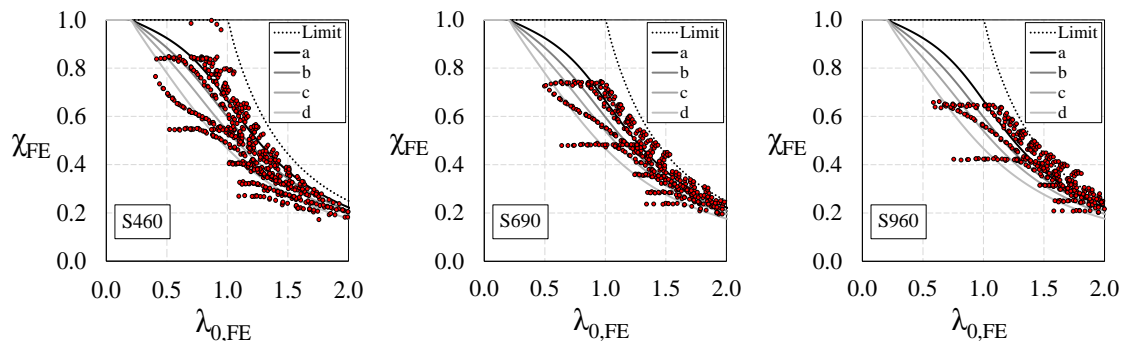
185



(a) $d_o/H=0.65$



(b) $d_o/H=0.75$



(c) $d_o/H=0.85$

186

Fig. 9: d_o/H ratio vs. buckling curves of EC3

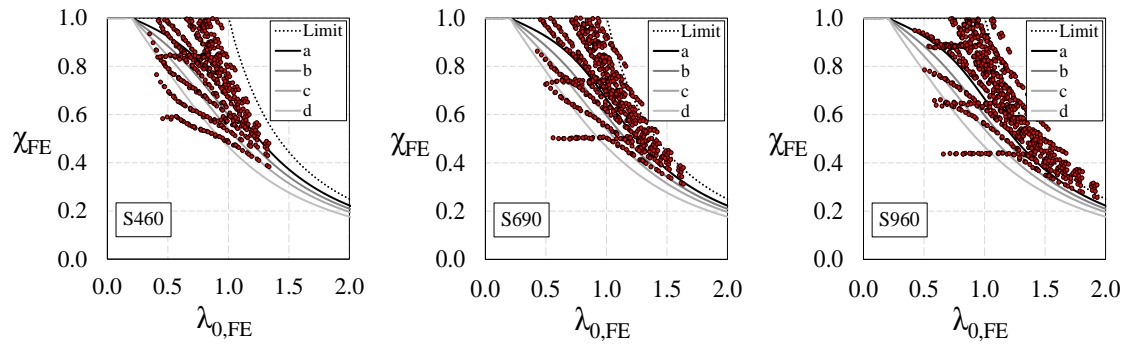
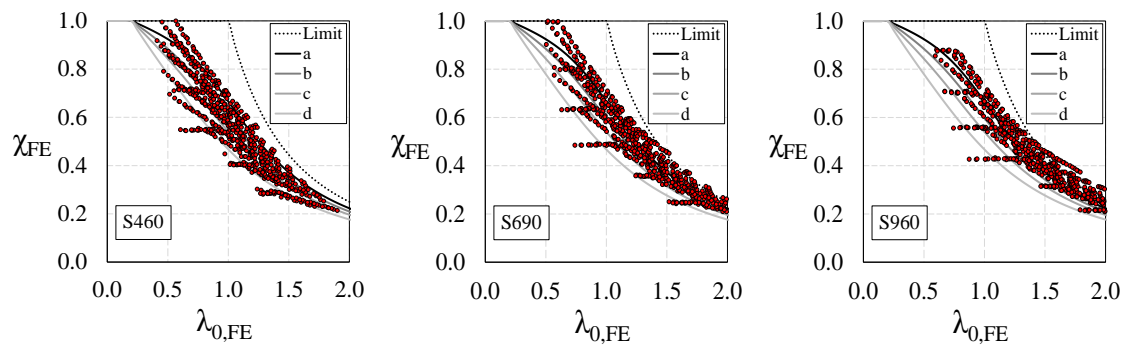
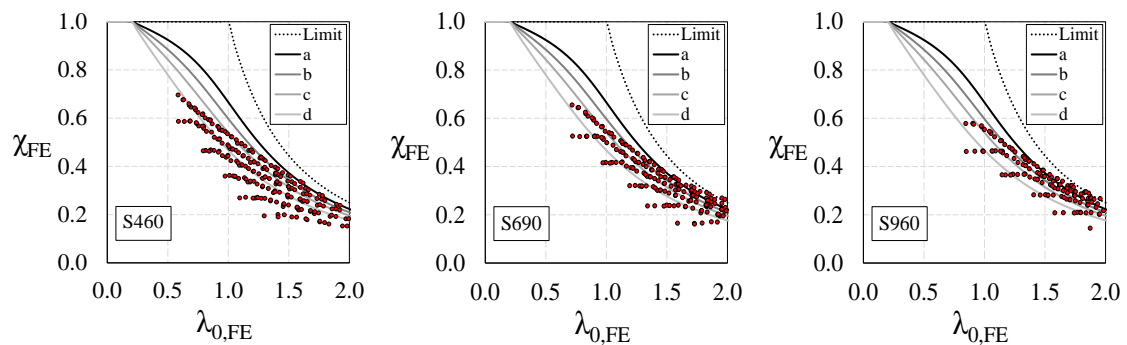
187

188

189

190

191

(a) $R/d_o=0.1$ (b) $R/d_o=0.2$ (c) $R/d_o=0.3$ Fig. 10: R/d_o ratio vs. buckling curves of EC3

192

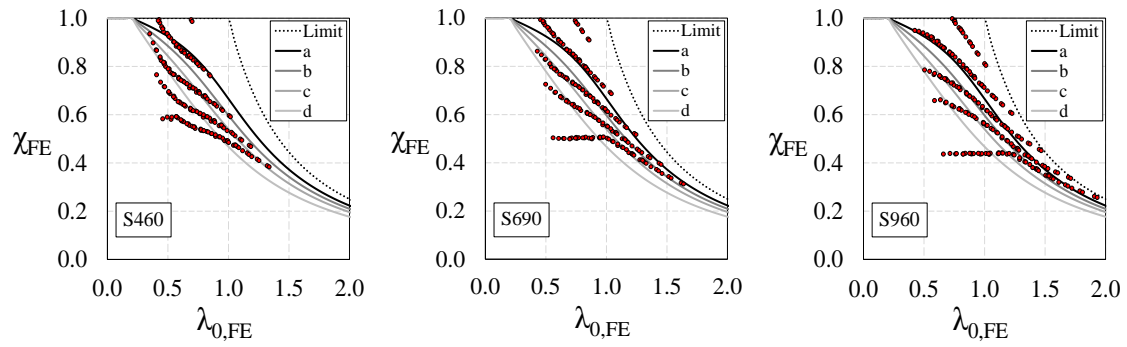
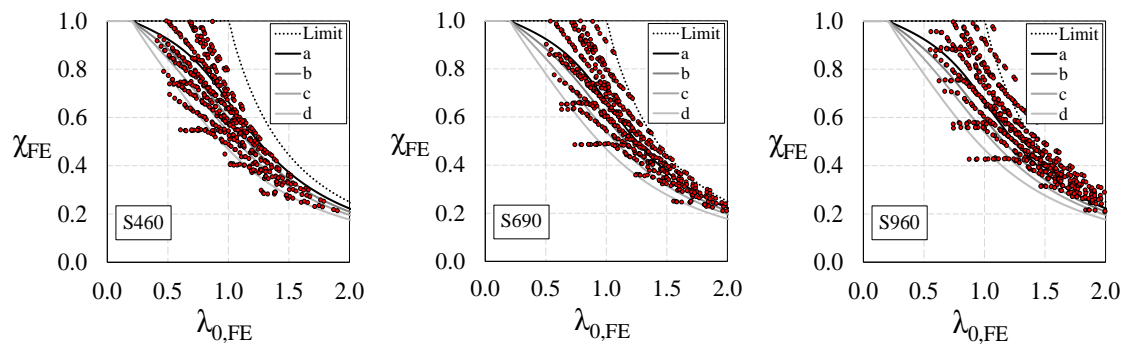
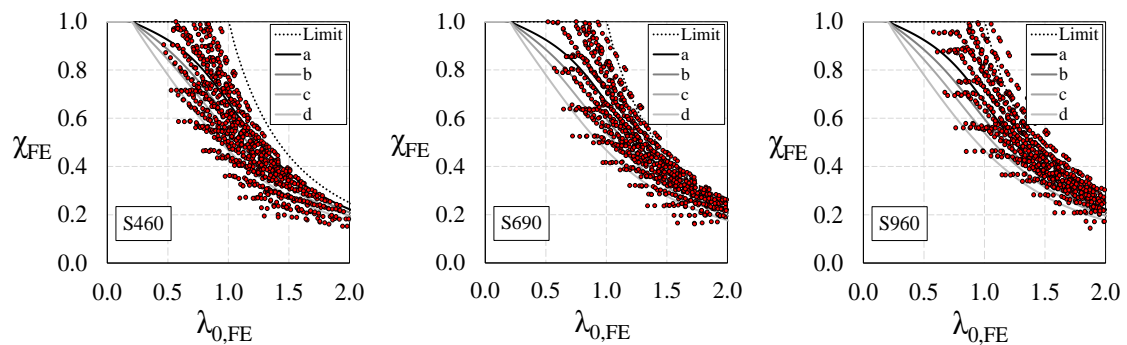
193

194

195

196

197

(a) $w/d_o=0.25$ (b) $w/d_o=0.45$ (c) $w/d_o=0.65$

198

Fig. 11: w/d_o ratio vs. buckling curves of EC3

199

200

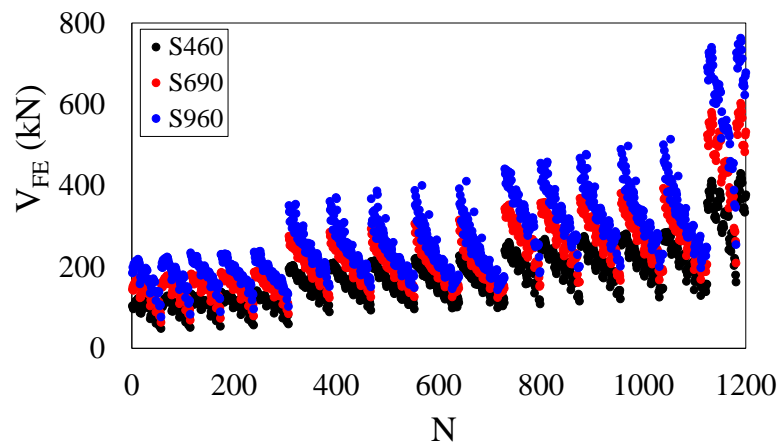
201

202

203

204 5.1 *Yield strength*

205 From the analyses carried out, it was possible to observe the influence
 206 of the yield strength on the web-post buckling resistance. **Fig. 12** illustrates
 207 this behaviour, considering 1,200 data points, as an example. It is notable
 208 that the greater the yield strength, the greater the web-post buckling
 209 resistance. In this context, a comparative analysis can be made through the
 210 ratios V_{S690}/V_{S460} , V_{S960}/V_{S460} , and V_{S960}/V_{S690} considering the capacity of all
 211 finite element models. The S690 steel grade in relation to the S460 showed a
 212 minimum and maximum gain in capacity of 11% and 49%, respectively, with
 213 the average value of the V_{S690}/V_{S460} equal to 1.33. Regarding S960 steel grade
 214 compared to the S460, showed 24% and 99%, respectively, of a minimum and
 215 maximum gain in capacity. The average value of the V_{S960}/V_{S460} is equal to
 216 1.61. Finally, by comparing the S960 and S690 steel grades, a minimum and
 217 maximum gain in capacity of 1% and 57%, respectively, was observed. The
 218 average value of the V_{S960}/V_{S690} is equal to 1.21.



219

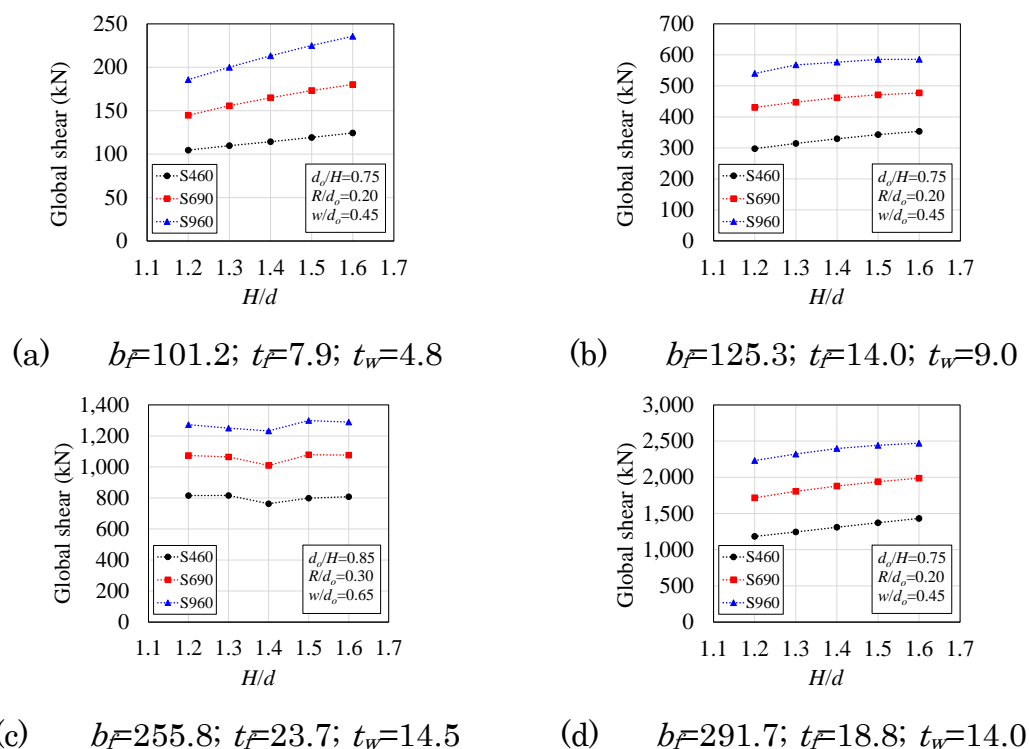
220 Fig. 12: Capacity of the web-post made of high-strength steels

221

222

223 5.2 H/d ratio

224 **Fig. 13** provides the relationship between global shear capacity and H/d
 225 ratio for three classes of high-strength steel (S460, S690 and S960). The H/d
 226 ratio was increased from 1.2 to 1.6 in increments of 0.1. **Fig. 13a**, **Fig. 13b**,
 227 **Fig. 13c** and **Fig. 13d** show the impact of b_f , t_f and t_w , as parameters increase,
 228 there is an increase in resistance. Furthermore, it shows that as the
 229 expansion factor increases, so does the global shear capacity for all strength
 230 classes examined. When increasing the H/d ratio and keeping the other
 231 geometric parameters constant, there was an increase in global shear
 232 resistance. This can be explained by the increase in the steel area.

233 Fig. 13: Influence of H/d ratio on capacity (dimensions in mm)

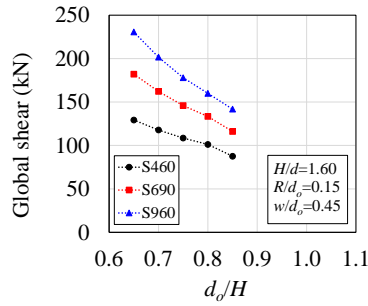
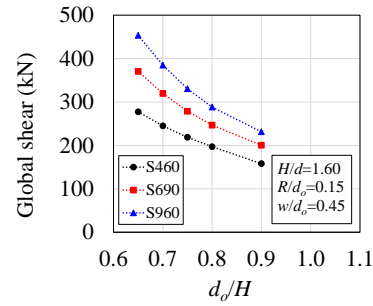
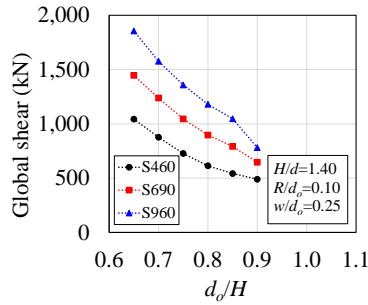
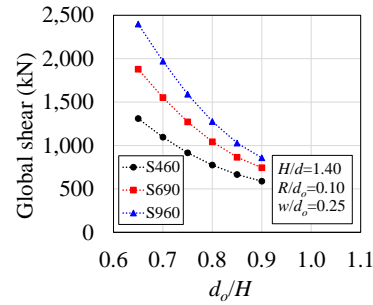
234 **Fig. 8** provided the EC3 buckling curves, and shows how the increase
 235 in the expansion ratio results in samples exceeding the resistance limit
 236 values. The impact of increasing the ratio of opening height over the distance

237 between flanges geometric centres after the castellation process (d_o/H), the
238 ratio of opening radius over opening height (R/d_o) and the ratio of opening
239 width over opening height (w/d_o) can be seen in **Fig. 13c**. The trend showed a
240 slight decrease in global shear capacity as the expansion factor increased from
241 1.2 to 1.4, thereafter, an increase in global shear capacity from 1.4 to 1.6. It
242 can be assumed an increase in d_o and R will increase d_o/H and R/d_o
243 respectively, therefore, decreasing the height of the tee section and decreasing
244 the resistance to global shear capacity.

245

246 5.3 d_o/H ratio

247 **Fig. 14** provides the relationship between global shear capacity and the
248 ratio of opening height over the distance between flanges geometric centres
249 after the castellation process (d_o/H) for the three classes of high-strength steel
250 (S460, S690 and S960). Results clearly show that an increase in d_o/H will
251 reduce the global shear capacity. This is due to the reduction in height of the
252 tee section as stated in section 5.2. Furthermore, when reviewing **Fig. 9**,
253 which provides d_o/H ratio vs. buckling curves of EC3, it can be seen that as
254 d_o/H increases there is a decrease in capacity resistance. It also showed
255 similar trends noted by Ferreira et al. [16], in which tee sections experienced
256 instability phenomena before reaching the yield strength for d_o/H ratios of
257 0.75 and 0.85 and $\lambda_0 < 1.0$.

(a) $b_f=101.2$; $t_f=7.9$; $t_w=4.8$ (b) $b_f=102.4$; $t_f=10.8$; $t_w=6.6$ (c) $b_f=196.7$; $t_f=26.3$; $t_w=15.3$ (d) $b_f=291.7$; $t_f=18.8$; $t_w=14.0$

258

Fig. 14: Influence of d_o/H ratio on capacity (dimensions in mm)

259

260 5.4 R/d_o ratio

261 The relationship between the global shear capacity and the ratio of
 262 opening radius over opening height (R/d_o) can be seen in **Fig. 15**, for the three
 263 classes of high-strength steel (S460, S690 and S960). R/d_o increased from 0.1
 264 to 0.3 in increments of 0.5. **Fig. 15a** and **Fig. 15b** show that as the ratio
 265 increases to 0.15, there is a slight increase in the global shear, thereafter, as
 266 the ratio increases the capacity decreases. A similar trend can be noted in **Fig.**
 267 **15b**. **Fig. 15c** shows that there is a negative relationship followed by a positive
 268 correlation. This shows that the beams are potentially sensitive to an increase
 269 in d_o/H .

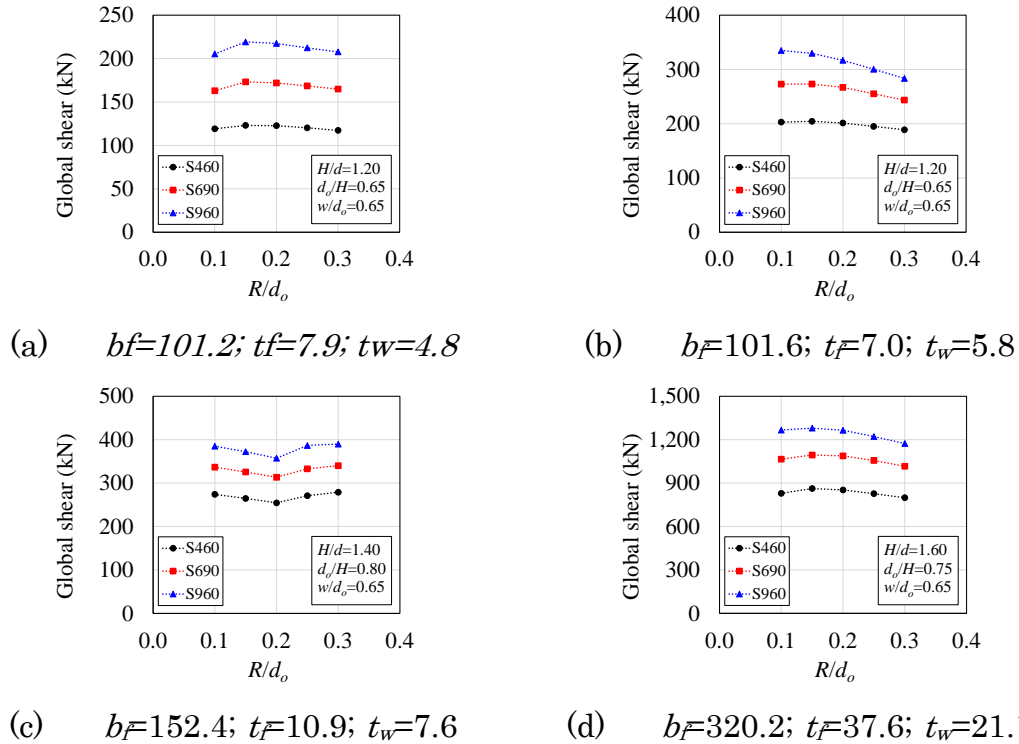


Fig. 15: Influence of R/d_o ratio on capacity (dimensions in mm)

270

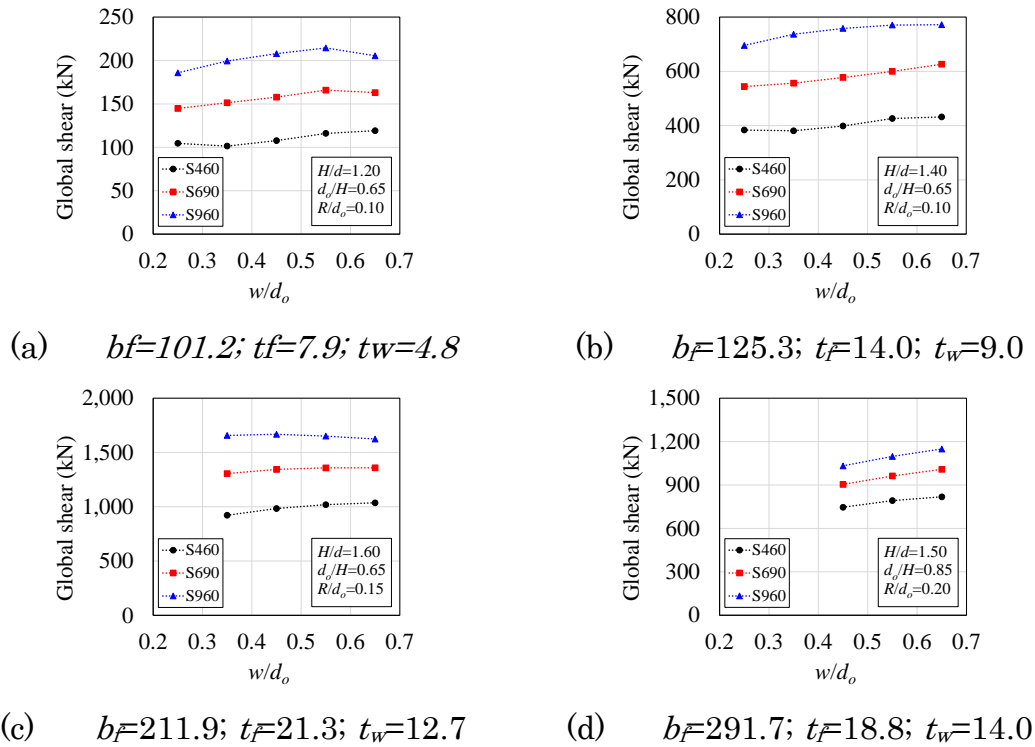
271 As expected, as the opening radius increases so does R/d_o , resulting in
 272 a decreased resistance. However, from **Fig. 10** which provided R/d_o vs
 273 buckling curves for EC3, it is observed that the global shear is sensitive to
 274 R/d_o . As R/d_o is increased from 0.1 to 0.3, the resistance moves from exceeding
 275 the limit value to falling below or close to buckling curves d and c ,
 276 respectively. Furthermore, it can be concluded that tee sections experienced
 277 instability phenomena before reaching the yield strength for R/d_o ratios of 0.1,
 278 0.2 and 0.3 at $\lambda_0 < 1.0$, $\lambda_0 < 1.75$ and $\lambda_0 < 2.0$, respectively.

279

280 5.5 w/d_o ratio

281 **Fig. 16** provides the relationship between global shear capacity and the
 282 ratio of opening width over opening height (w/d_o) for three classes of high-
 283 strength steel (S460, S690 and S960). Results show that an increase in w/d_o

284 increases the global shear. This is further verified by **Fig. 11**, which shows
 285 that as w/d_o increases, the resistance moves closer to exceeding the limits of
 286 the buckling curves of EC3.



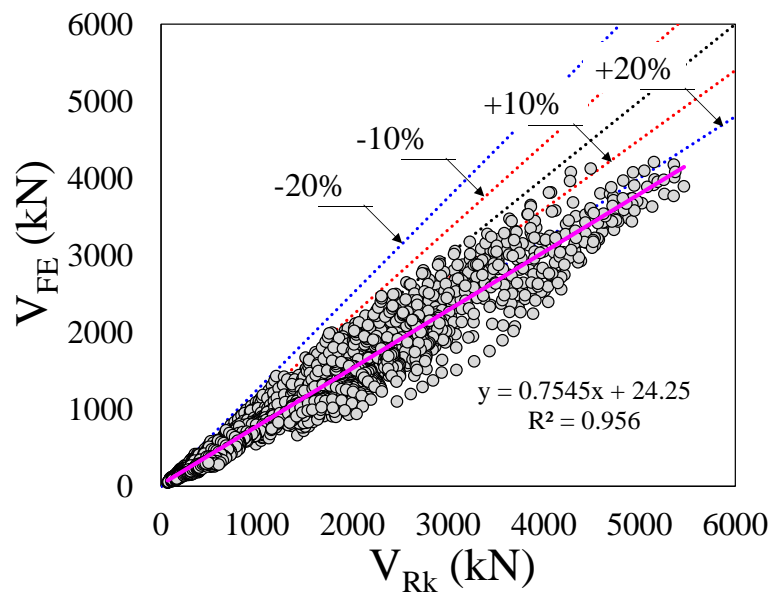
287 Fig. 16: Influence of w/d_o ratio on capacity (dimensions in mm)

288

289 6. Comparison with design equations for normal strength steel

290 In this section, the results of the finite element models are compared
 291 with the equation previously proposed by Ferreira et al. [16], considering
 292 normal strength steels (**Eqs. 1-10**), as shown in **Fig. 17**. In Appendix A an
 293 example of verification is shown. On analysis of the V_{FE}/V_{RK} ratio as a
 294 comparison parameter, values of 0.88, 6.99% and 0.49% were verified for the
 295 S460 class, considering the average, standard deviation and variance,
 296 respectively. The maximum relative error was 33.71%, while the minimum
 297 relative error was -19.05%. In relation to the S690 class, the statistical values

298 presented for the average, standard deviation and variance were,
 299 respectively, equal to 0.78, 8.52% and 0.73%. In this context, the maximum
 300 and minimum relative errors were equal to 46.1% and -13.34%. Finally, in
 301 relation to the S960 class, the average, standard deviation and variance
 302 values were equal to 0.70, 9.31% and 0.87%, respectively, and the maximum
 303 and minimum relative errors were equal to 55.29% and -7.34%. **Table 1** shows
 304 the statistical values, considering the general analysis.



305

306 Fig. 17: FEM vs. Design equation for common strength steels

307 Table 1: Statistical analysis for design equation for normal strength steels

Analysis	Value
R ² (Regression)	0.9560
RMSE (Root Mean Square Error) (kN)	99.5767
MAE (Mean Absolute Error) (kN)	73.2603
Minimum relative error	-16.00
Maximum relative error	123.70
Average (FEM/Predicted)	0.791
S.D.	11.20%
Var.	1.25%

308

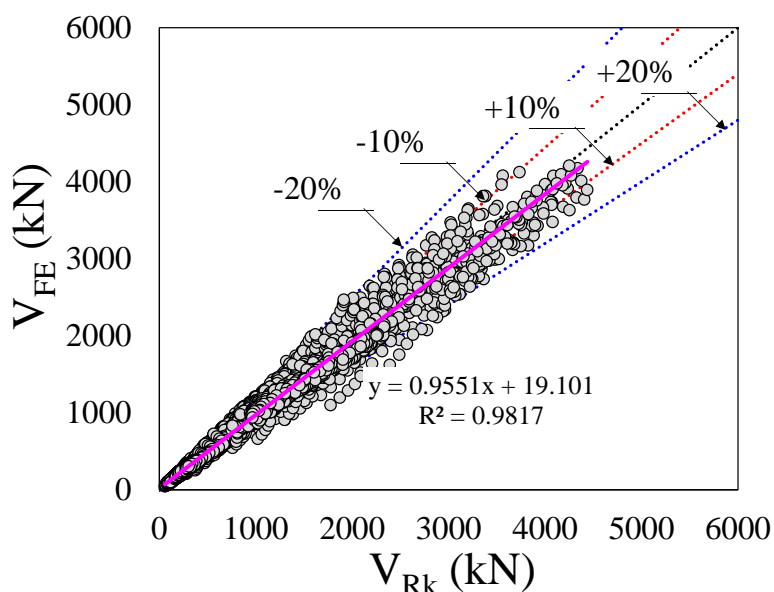
309

310 **7. Design recommendation**

311 The calculation procedure proposed previously by Ferreira et al. [16]
 312 considered normal strength of steels. In this context, to adapt the high-
 313 strength steel models in the calculation of the web-post buckling resistance
 314 (Eqs. 1-10), a K_{HSS} factor is proposed, according to Eqs (13-14). Fig. 18 and
 315 Table 2 show the statistical analysis with the application of the new factor.
 316 With this, it is possible to affirm that the new proposal presented is applicable
 317 for HSS. In the next section, a reliability analysis is applied according to
 318 Annex D EN 1990 [40]. It is worth to note that the coefficients of the Eq. (14)
 319 are obtained from the statistical analysis, hence, the proposed equation is
 320 limited to the geometric parameters illustrated in Table 3.

$$\sigma_{Rk} = K_{HSS} \chi f_y \quad (13)$$

$$K_{HSS} = -1.45 + 1.606 \left(\frac{H}{d_o} \right) + 0.333 \left(\frac{s}{s-w} \right) - 0.905 \left(\frac{s}{d_o} \right) + 0.213 \left(\frac{w}{d_o} \right) - 0.004 \left(\frac{d_o}{t_w} \right) + 0.489 \lambda_0 \quad (14)$$



321

322

Fig. 18: FEM vs. Design equation for high-strength steel

323 Table 2: Statistical analysis for design equation for high-strength steel

Analysis	Value
R ² (Regression)	0.9817
RMSE (Root Mean Square Error) (kN)	58.8588
MAE (Mean Absolute Error) (kN)	35.7895
Minimum relative error	-22.61
Maximum relative error	61.05
Average (FEM/Predicted)	0.986
S.D.	8.32%
Var.	0.69%

324

325 Table 3: Parameters limitation (in mm and MPa)

Parameter	Minimum	Maximum
Flange width (b_f)	101.2	320.2
Flange thickness (t_f)	7.0	37.6
Distance between flanges geometric centres (H)	213.4	1335.8
Web thickness (t_w)	4.8	21.1
Opening height (d_o)	138.7	1202.3
Opening width (w)	34.7	781.5
Opening radius (R)	13.9	360.7
Yield strength (f_y)	460	960

326

327 **8. A statistical evaluation based on Annex D EN 1990**

328 In this section, a statistical analysis based on Annex D EN 1990 (2002)
329 [40] has been conducted to assess the reliability of the proposed formulation
330 and propose a partial safety factor for web-post buckling resistance. The
331 statistical evaluation of the proposed prediction model is done herein based
332 on the generated numerical results.

333 **Table 4** illustrates the key statistical parameters, including the
334 number of data, n , the design fractile factor (ultimate limit state), $k_{d,n}$, the
335 average ratio of numerical to resistance model predictions based on the least
336 squares fit to the data, \bar{b} , the combined coefficient of variation incorporating
337 both resistance model and basic variable uncertainties, V_r , and the partial

338 safety factor for WPB resistance γ_{M0} . The COV of geometric properties and
 339 the high-strength steel material properties were assumed equal to 0.02 and
 340 0.0055 [35]. The material over-strength of high-strength steel was taken
 341 equal to 1.135 [35]. The COV between the experimental and the numerical
 342 results, which was equal to 0.0133, was also considered. Performing First
 343 Order Reliability Method (FORM) in accordance with the Eurocode target
 344 reliability requirements, the partial factors γ_{M0} were evaluated. For S460,
 345 S690 and S960 the partial factors γ_{M0} were 1.03, 1.05 and 1.09, respectively.
 346 Furthermore, considering all HSS grades used in this study, the partial factor
 347 was 1.07.

348 Table 4: Summary of the reliability analysis for the proposed formulation

Grade	n	\bar{b}	$k_{d,n}$	V_r	γ_{M0}
S460	3588	1.013	3.04	0.102	1.03
S690	3588	0.994	3.04	0.102	1.05
S960	3588	0.961	3.04	0.103	1.09
All	10764	0.98	3.04	0.104	1.07

349

350 Concluding remarks

351 This paper is the first study of high-strength steel perforated steel
 352 beams with elliptically-based web openings. In particular, the web-post
 353 buckling is studied, and a resistance equation based on the truss model
 354 according to EUROCODE 3 is presented. A comprehensive parametric study
 355 of 13,500 FE models is carried out, considering the key geometric parameters
 356 that influence the web-post buckling resistance. A reliability analysis is also
 357 presented based on Annex D EN 1990 (2002). The following concluding
 358 remarks are summarised as:

- 359 1. The yield strength influenced the web-post buckling resistance. It was
360 found that the greater the yield strength, the greater the web-post
361 buckling resistance.
- 362 2. As the expansion factor (H/d ratio) increases, the global shear capacity
363 for all three strength classes increases because of the increased in the
364 steel area and therefore an increase in global shear resistance.
- 365 3. Decreasing the height of the tee section, so does the resistance to global
366 shear capacity.
- 367 4. As the web opening radius increases, the R/d_o also increases, resulting
368 in a decreased resistance. However, the global shear is sensitive to
369 R/d_o .
- 370 5. The increase in w/d_o increases the global shear. As w/d_o increases, the
371 resistance moves closer to exceeding the limits of the buckling curves
372 of EC3.

373

374 **Appendix A: Application example**

375 Check the web-post buckling resistance of perforated high-strength
376 steel beams with elliptically-based web openings made of S460 and UB
377 457x152x52 section, considering the formulation for common and high-
378 strength steel. Table A.1 presents the geometric characteristics of the section
379 after the castellation process.

380

381

382

383 Table A.1: geometric characteristics

b_f (mm): 152.40	t_w (mm): 7.60	R (mm): 105.25
t_f (mm): 10.90	d_o (mm): 526.27	s (mm): 499,95
H (mm): 584.74	w (mm): 289.45	

384

385 For common steel:

386 - Web-post effective length and slenderness factor (Eqs 1-3):

$$387 \quad k = 0.516 - 0.288 \left(\frac{H}{d_o} \right) + 0.062 \left(\frac{s}{s-w} \right) + 2.384 \left(\frac{s}{d_o} \right) - 2.906 \left(\frac{w}{d_o} \right)$$

$$388 \quad \rightarrow k = 0.516 - 0.288 \left(\frac{584.74}{526.27} \right) + 0.062 \left(\frac{499,95}{499,95 - 289.45} \right) + 2.384 \left(\frac{499,95}{526.27} \right)$$

$$389 \quad \quad \quad - 2.906 \left(\frac{289.45}{526.27} \right)$$

$$390 \quad \rightarrow k = 1.01$$

391 Thus:

$$392 \quad l_{eff} = k \sqrt{\left(\frac{d_o - 2R}{2} \right)^2 + \left(\frac{s}{2} - R \right)^2}$$

$$393 \quad \rightarrow l_{eff} = 1.01 \sqrt{\left(\frac{526.27 - 2 \times 105.25}{2} \right)^2 + \left(\frac{499,95}{2} - 105.25 \right)^2}$$

$$394 \quad \rightarrow l_{eff} = 216.26 \text{ mm}$$

395 Finally:

$$396 \quad \lambda_w = \frac{l_{eff} \sqrt{12}}{t_w} = \frac{216.26 \sqrt{12}}{7.60} = 98.57$$

397

398 - EC3 reduction factor (Eqs 4-7):

399 Critical shear stress in the web-post:

$$400 \quad f_{cr,w} = \frac{\pi^2 E}{\lambda_w^2} = \frac{\pi^2 \times 200000}{98.57^2} = 203.15 \text{ MPa}$$

401 The reduced slenderness factor:

$$402 \quad \lambda_0 = \sqrt{\frac{f_y}{f_{cr,w}}} = \sqrt{\frac{460}{203.15}} = 1.50$$

403 Imperfection factor:

$$404 \quad \phi = 0.5[1 + 0.49(\lambda_0 - 0.2) + \lambda_0^2] = 0.5[1 + 0.49(1.50 - 0.2) + 1.50^2] = 1.95$$

405 Finally, the reduction factor

$$406 \quad \chi = \frac{1}{\phi + \sqrt{\phi^2 - \lambda_0^2}} = \frac{1}{1.95 + \sqrt{1.95^2 - 1.50^2}} = 0.31$$

407

408 - Web-post buckling resistance (Eqs 8-10):

$$409 \quad K = -1.318 + 1.790 \left(\frac{H}{d_o}\right) + 0.413 \left(\frac{s}{s-w}\right) - 1.926 \left(\frac{s}{d_o}\right) + 0.937 \left(\frac{w}{d_o}\right) - 0.02 \left(\frac{d_o}{t_w}\right)$$

$$410 \quad + 1.412\lambda_0$$

$$411 \quad \rightarrow K = -1.318 + 1.790 \left(\frac{584.74}{526.27}\right) + 0.413 \left(\frac{499,95}{499,95 - 289.45}\right) - 1.926 \left(\frac{499,95}{526.27}\right)$$

$$412 \quad + 0.937 \left(\frac{289.45}{526.27}\right) - 0.02 \left(\frac{526.27}{7.6}\right) + 1.412 \times 1.50$$

$$413 \quad \rightarrow K = 1.08$$

414 Thus, the ultimate stress can be calculated:

$$415 \quad \sigma_{Rk} = K\chi f_y = 1.08 \times 0.31 \times 460 = 155.1 \text{ MPa}$$

416 Finally, the web-post buckling resistance is predicted:

$$417 \quad V_{Rk} = \sigma_{Rk} t_w (s - w) = 155.1 \times 7.6 (499,95 - 289.45) = 248.13 \text{ kN}$$

418 For high-strength steel:

419 The procedure is similar to that used in common steel, considering Eqs.

420 (1-7) shown previously.

421 -Web-post buckling resistance (Eqs 13-14):

$$\begin{aligned}
422 \quad K_{HSS} &= -1.45 + 1.606 \left(\frac{H}{d_o} \right) + 0.333 \left(\frac{s}{s-w} \right) - 0.905 \left(\frac{s}{d_o} \right) + 0.213 \left(\frac{w}{d_o} \right) \\
423 \quad &\quad - 0.004 \left(\frac{d_o}{t_w} \right) + 0.489 \lambda_0 \\
424 \quad \rightarrow K_{HSS} &= -1.45 + 1.606 \left(\frac{584.74}{526.27} \right) + 0.333 \left(\frac{499.95}{499.95 - 289.45} \right) - 0.905 \left(\frac{499.95}{526.27} \right) \\
425 \quad &\quad + 0.213 \left(\frac{289.45}{526.27} \right) - 0.004 \left(\frac{526.27}{7.6} \right) + 0.489 \times 1.50 \\
426 \quad \rightarrow K_{HSS} &= 0.84
\end{aligned}$$

427 Thus, the ultimate stress can be calculated:

$$428 \quad \sigma_{Rk} = K_{HSS} \chi f_y = 0.84 \times 0.31 \times 460 = 119.78 \text{ MPa}$$

429 Finally, the web-post buckling resistance is predicted:

$$430 \quad V_{Rk} = \sigma_{Rk} t_w (s - w) = 119.78 \times 7.6 (499.95 - 289.45) = 193.85 \text{ kN}$$

431

432 Table A.2 shows the comparison between the equations with the
433 prediction of the finite element method.

434 Table A.2: Comparative analysis

Common steel method	High-strength steel method	Finite element method
248.13 kN	193.85 kN	205.81 kN

435

436 References

- 437 [1] F.P.V. Ferreira, C.H. Martins, S. De Nardin, Advances in composite
438 beams with web openings and composite cellular beams, J Constr Steel
439 Res. 172 (2020) 106182. <https://doi.org/10.1016/j.jcsr.2020.106182>.
- 440 [2] R.M.M. Lawson, J. Lim, S.J.J. Hicks, W.I.I. Simms, Design of composite
441 asymmetric cellular beams and beams with large web openings, J

- 442 Constr Steel Res. 62 (2006) 614–629.
443 <https://doi.org/10.1016/j.jcsr.2005.09.012>.
- 444 [3] F.P.V. Ferreira, R. Shamass, V. Limbachiya, K.D. Tsavdaridis, C.H.
445 Martins, Lateral–torsional buckling resistance prediction model for
446 steel cellular beams generated by Artificial Neural Networks (ANN),
447 Thin-Walled Structures. 170 (2022) 108592.
448 <https://doi.org/10.1016/j.tws.2021.108592>.
- 449 [4] E. Ellobody, Nonlinear analysis of cellular steel beams under combined
450 buckling modes, Thin-Walled Structures. 52 (2012) 66–79.
451 <https://doi.org/10.1016/j.tws.2011.12.009>.
- 452 [5] K.M. El-Sawy, A.M.I. Sweedan, M.I. Martini, Moment gradient factor
453 of cellular steel beams under inelastic flexure, J Constr Steel Res. 98
454 (2014) 20–34. <https://doi.org/10.1016/j.jcsr.2014.02.007>.
- 455 [6] P. Panedpojaman, W. Sae-Long, T. Chub-Uppakarn, Cellular beam
456 design for resistance to inelastic lateral-torsional buckling, Thin-Walled
457 Structures. 99 (2016) 182–194.
458 <https://doi.org/10.1016/j.tws.2015.08.026>.
- 459 [7] L.F. Grilo, R.H. Fakury, A.L.R. de Castro e Silva, G. de S. Veríssimo,
460 Design procedure for the web-post buckling of steel cellular beams, J
461 Constr Steel Res. 148 (2018) 525–541.
462 <https://doi.org/10.1016/j.jcsr.2018.06.020>.
- 463 [8] K.D. Tsavdaridis, C. D’Mello, Web buckling study of the behaviour and
464 strength of perforated steel beams with different novel web opening

- 465 shapes, *J Constr Steel Res.* 67 (2011) 1605–1620.
466 <https://doi.org/10.1016/j.jcsr.2011.04.004>.
- 467 [9] V. Limbachiya, R. Shamass, Application of Artificial Neural Networks
468 for web-post shear resistance of cellular steel beams, *Thin-Walled
469 Structures.* 161 (2021) 107414.
470 <https://doi.org/10.1016/j.tws.2020.107414>.
- 471 [10] D. Kerdal, D.A. Nethercot, Failure modes for castellated beams, *J
472 Constr Steel Res.* 4 (1984) 295–315. [https://doi.org/10.1016/0143-
473 974X\(84\)90004-X](https://doi.org/10.1016/0143-974X(84)90004-X).
- 474 [11] K.D. Tsavdaridis, Structural performance of perforated steel beams
475 with novel web openings and with partial concrete encasement,
476 *Doctoral Thesis, City University London,* 2010.
477 <https://openaccess.city.ac.uk/id/eprint/11660/>.
- 478 [12] K.D. Tsavdaridis, C. D’Mello, FE Investigation of Perforated Sections
479 with Standard and Non-Standard Web Opening Configurations and
480 Sizes, in: S.L. Chan (Ed.), *6th International Conference on Advances In
481 Steel Structures*, Hong Kong Institute of Steel Construction, Hong
482 Kong, China, 2009: pp. 213–220.
- 483 [13] K.D. Tsavdaridis, C. D’Mello, Vierendeel Bending Study of Perforated
484 Steel Beams with Various Novel Web Opening Shapes through
485 Nonlinear Finite-Element Analyses, *Journal of Structural Engineering.*
486 138 (2012) 1214–1230. [https://doi.org/10.1061/\(asce\)st.1943-
487 541x.0000562](https://doi.org/10.1061/(asce)st.1943-541x.0000562).

- 488 [14] K.D. Tsavdaridis, J.J. Kingman, V. V. Toropov, Application of
489 structural topology optimisation to perforated steel beams, *Comput*
490 *Struct.* 158 (2015) 108–123.
491 <https://doi.org/10.1016/j.compstruc.2015.05.004>.
- 492 [15] K.D. Tsavdaridis, C. D’Mello, Optimisation of novel elliptically-based
493 web opening shapes of perforated steel beams, *J Constr Steel Res.* 76
494 (2012) 39–53. <https://doi.org/10.1016/j.jcsr.2012.03.026>.
- 495 [16] F.P.V. Ferreira, R. Shamass, L.F.P. Santos, V. Limbachiya, K.D.
496 Tsavdaridis, EC3 design of web-post buckling resistance for perforated
497 steel beams with elliptically-based web openings, *Thin-Walled*
498 *Structures.* 175 (2022) 109196.
499 <https://doi.org/10.1016/j.tws.2022.109196>.
- 500 [17] European committee for standardization, EN 1993-1-1: Eurocode 3 –
501 Design of steel structures – Part 1-1: General rules and rules for
502 buildings, (2002).
- 503 [18] K.D. Tsavdaridis, C. D’Mello, Structural beam, GB 2492176, 2012.
- 504 [19] C. Miki, K. Homma, T. Tominaga, High strength and high performance
505 steels and their use in bridge structures, *J Constr Steel Res.* 58 (2002)
506 3–20. [https://doi.org/10.1016/S0143-974X\(01\)00028-1](https://doi.org/10.1016/S0143-974X(01)00028-1).
- 507 [20] M. Veljkovic, B. Johansson, Design of hybrid steel girders, *J Constr*
508 *Steel Res.* 60 (2004) 535–547. [https://doi.org/10.1016/S0143-](https://doi.org/10.1016/S0143-974X(03)00128-7)
509 [974X\(03\)00128-7](https://doi.org/10.1016/S0143-974X(03)00128-7).

- 510 [21] R. Bjorhovde, Development and use of high performance steel, *J Constr*
511 *Steel Res.* 60 (2004) 393–400. [https://doi.org/10.1016/S0143-](https://doi.org/10.1016/S0143-974X(03)00118-4)
512 [974X\(03\)00118-4](https://doi.org/10.1016/S0143-974X(03)00118-4).
- 513 [22] A. WHEELER, B. RUSSELL, Behaviour and design of webs in high
514 strength steel under flexural loading, in: *Fourth International*
515 *Conference on Advances in Steel Structures*, Elsevier, 2005: pp. 137–
516 142. <https://doi.org/10.1016/B978-008044637-0/50018-4>.
- 517 [23] G. Shi, X. Zhu, H. Ban, Material properties and partial factors for
518 resistance of high-strength steels in China, *J Constr Steel Res.* 121
519 (2016) 65–79. <https://doi.org/10.1016/j.jcsr.2016.01.012>.
- 520 [24] B. Karabulut, G. Ferraz, B. Rossi, Lifecycle cost assessment of high
521 strength carbon and stainless steel girder bridges, *J Environ Manage.*
522 277 (2021) 111460. <https://doi.org/10.1016/j.jenvman.2020.111460>.
- 523 [25] K. Mela, M. Heinisuo, Weight and cost optimization of welded high
524 strength steel beams, *Eng Struct.* 79 (2014) 354–364.
525 <https://doi.org/10.1016/j.engstruct.2014.08.028>.
- 526 [26] Dassault Systèmes Simulia, Abaqus 6.18, (2016).
- 527 [27] R.M. Lawson, S.J. Hicks, Design of composite beams with large web
528 openings. SCI P355., The Steel Construction Institute, 2011.
- 529 [28] W. Zaarour, R. Redwood, Web Buckling in Thin Webbed Castellated
530 Beams, *Journal of Structural Engineering.* 122 (1996) 860–866.
531 [https://doi.org/10.1061/\(ASCE\)0733-9445\(1996\)122:8\(860\)](https://doi.org/10.1061/(ASCE)0733-9445(1996)122:8(860)).
- 532 [29] P. Panedpojaman, T. Thepchatri, S. Limkatanyu, Novel design
533 equations for shear strength of local web-post buckling in cellular

- 534 beams, Thin-Walled Structures. 76 (2014) 92–104.
535 <https://doi.org/10.1016/j.tws.2013.11.007>.
- 536 [30] K.D. Tsavdaridis, G. Galiatsatos, Assessment of cellular beams with
537 transverse stiffeners and closely spaced web openings, Thin-Walled
538 Structures. 94 (2015) 636–650.
539 <https://doi.org/10.1016/j.tws.2015.05.005>.
- 540 [31] S. Durif, A. Bouchaïr, O. Vassart, Experimental and numerical
541 investigation on web-post specimen from cellular beams with sinusoidal
542 openings, Eng Struct. 59 (2014) 587–598.
543 <https://doi.org/10.1016/j.engstruct.2013.11.021>.
- 544 [32] F.P.V. Ferreira, K.D. Tsavdaridis, C.H. Martins, S. De Nardin,
545 Ultimate strength prediction of steel–concrete composite cellular beams
546 with PCHCS, Eng Struct. 236 (2021) 112082.
547 <https://doi.org/10.1016/j.engstruct.2021.112082>.
- 548 [33] F.P.V. Ferreira, K.D. Tsavdaridis, C.H. Martins, S. De Nardin,
549 Buckling and post-buckling analyses of composite cellular beams,
550 Compos Struct. 262 (2021).
551 <https://doi.org/10.1016/j.compstruct.2021.113616>.
- 552 [34] F.P.V. Ferreira, K.D. Tsavdaridis, C.H. Martins, S. De Nardin,
553 Composite action on web-post buckling shear resistance of composite
554 cellular beams with PCHCS and PCHCSCT, Eng Struct. 246 (2021)
555 113065. <https://doi.org/10.1016/j.engstruct.2021.113065>.

- 556 [35] R. Shamass, F. Guarracino, Numerical and analytical analyses of high-
557 strength steel cellular beams: A discerning approach, *J Constr Steel*
558 *Res.* 166 (2020) 105911. <https://doi.org/10.1016/j.jcsr.2019.105911>.
- 559 [36] X. Yun, L. Gardner, Stress-strain curves for hot-rolled steels, *J Constr*
560 *Steel Res.* 133 (2017) 36–46. <https://doi.org/10.1016/j.jcsr.2017.01.024>.
- 561 [37] F.P.V. Ferreira, A. Rossi, C.H. Martins, Lateral-torsional buckling of
562 cellular beams according to the possible updating of EC3, *J Constr Steel*
563 *Res.* 153 (2019) 222–242. <https://doi.org/10.1016/j.jcsr.2018.10.011>.
- 564 [38] F.P.V. Ferreira, C.H. Martins, LRFD for Lateral-Torsional Buckling
565 Resistance of Cellular Beams, *International Journal of Civil*
566 *Engineering.* 18 (2020) 303–323. [https://doi.org/10.1007/s40999-019-](https://doi.org/10.1007/s40999-019-00474-7)
567 [00474-7](https://doi.org/10.1007/s40999-019-00474-7).
- 568 [39] R. Shamass, F.P.V. Ferreira, V. Limbachiya, L.F.P. Santos, K.D.
569 Tsavdaridis, Web-post buckling prediction resistance of steel beams
570 with elliptically-based web openings using Artificial Neural Networks
571 (ANN), *Thin-Walled Structures.* 180 (2022) 109959.
572 <https://doi.org/10.1016/j.tws.2022.109959>.
- 573 [40] European committee for standardization, EN 1990: Eurocode – Basis of
574 structural design, (n.d.).
575